

DroughtSet: Understanding Drought Through Spatial-Temporal Learning

Xuwei Tan¹, Qian Zhao², Yanlan Liu², Xueru Zhang¹

¹Department of Computer Science and Engineering, The Ohio State University

²School of Earth Sciences, The Ohio State University
{tan.1206, zhao.4243, liu.9367, zhang.12807}@osu.edu

Abstract

Drought is one of the most destructive and expensive natural disasters, severely impacting natural resources and risks by depleting water resources and diminishing agricultural yields. Under climate change, accurately predicting drought is critical for mitigating drought-induced risks. However, the intricate interplay among the physical and biological drivers that regulate droughts limits the predictability and understanding of drought, particularly at a subseasonal to seasonal (S2S) time scale. While deep learning has been demonstrated with potential in addressing climate forecasting challenges, its application to drought prediction has received relatively less attention. In this work, we propose a new dataset, DroughtSet, which integrates relevant predictive features and three drought indices from multiple remote sensing and reanalysis datasets across the contiguous United States (CONUS). DroughtSet specifically provides the machine learning community with a new real-world dataset to benchmark drought prediction models and more generally, time-series forecasting methods. Furthermore, we propose a spatial-temporal model *SPDrought* to predict and interpret S2S droughts. Our model learns from the spatial and temporal information of physical and biological features to predict three types of droughts simultaneously. Multiple strategies are employed to quantify the importance of physical and biological features for drought prediction. Our results provide insights for researchers to better understand the predictability and sensitivity of drought to biological and physical conditions. We aim to contribute to the climate field by proposing a new tool to predict and understand the occurrence of droughts and provide the AI community with a new benchmark to study deep learning applications in climate science. Resources are available at <https://github.com/osu-srml/DroughtSet>.

1 Introduction

Drought is among the most disastrous and costly natural hazards, affecting water resources, agricultural yields, heat waves, and ecosystem carbon sink (Cook, Mankin, and Anchukaitis 2018). Drought typically occurs under precipitation deficit, which is frequently accompanied by abnormally high temperatures and low humidity, leading to high evapotranspiration rates that quickly deplete soil moisture. As the global temperatures continue to increase, droughts are setting in quicker and becoming more intense and more frequent (Trenberth et al. 2014; Tripathy et al. 2023). In particular, recent

studies have highlighted the increasing frequency of S2S droughts, which initiate and intensify quickly at time scales from weeks to months, impairing ecosystem functions and challenging drought risk management practices (Pendergrass et al. 2020; Yuan et al. 2023). For example, precipitation deficits combined with record-high temperatures in 2012 led to rapid drought development across the central US within just two months, resulting in estimated losses exceeding \$30 billion.

Accurate prediction of droughts is crucial for societal preparedness and risk mitigation strategies (Otkin et al. 2018; White et al. 2017, 2022), but it still remains a significant challenge. Existing drought prediction models include data-driven (Bonaccorso, Cancelliere, and Rossi 2015; Santos, Portela, and Pulido-Calvo 2014; Wanders and Wada 2015), physically-based (Wanders and Wood 2016; Wang et al. 2009), and hybrid models (Wu et al. 2022b). While some of these models consider the interaction of biological drivers, their representations are generally simplified. In addition, most existing drought predictive models focused on single drought type, e.g. meteorological drought, hydrological drought, or ecological drought, while neglecting their joint behaviors. Tackling these drought prediction challenges require a robust and interpretable data-driven method that systematically integrates datasets of relevant climate and vegetation features to jointly predict multiple aspects of drought (AghaKouchak et al. 2022; Hao, Singh, and Xia 2018). However, most existing methods simplify or ignore dynamic interactions among different factors, which inhibits realizing the potential of artificial intelligence (AI) to improve drought prediction accuracy and advance mechanistic understanding of droughts. We discuss these in Appendix 6.2.

To address this research gap, we create a benchmark dataset, DroughtSet, by compiling climate, physical, and vegetation predictors that are relevant to drought initiation, development, and propagation from various remote sensing and reanalysis products across the contiguous United States (CONUS) during years 2003–2013. DroughtSet encompasses the wide diversity of climatic and ecological settings and includes frequent drought events in recent decades. Specifically, we collect and preprocess drought-related predictors as listed in Table 1 (e.g. precipitation, temperature, elevation, leaf area index), consisting of both static variables and dynamic variables with coordinates. We also compile three

drought indices: soil moisture drought measured by normalized surface soil moisture (Yuan et al. 2023), ecohydrological drought measured by the Evaporative Stress Index (ESI) (Otkin et al. 2014), and ecological drought measured by solar-induced chlorophyll fluorescence (SIF) (Mohammadi, Jiang, and Wang 2022). Collectively, DroughtSet can be used to benchmark multivariate forecasting, spatiotemporal forecasting, and irregular forecasting (learning from static variables). We hope to accelerate future research in drought predictions and benchmark deep learning-based methods by releasing this dataset.

In addition, we propose a multi-task SPatial-temporal framework for drought prediction on DroughtSet, referred to as *SPDrought*, which exploits the spatial-temporal interconnections within and across climate and vegetation features. It accounts for influences of nearby regions by aggregating temporal features with neighboring locations and learns from both static and dynamic features to predict three drought indices. Furthermore, we employ the Integrated Gradient (IG) method, as described in (Sundararajan, Taly, and Yan 2017), to interpret and quantify how these features influence drought development across CONUS. The results will serve as a data-driven benchmark, informing further research towards enhancing the mechanistic understanding and simulation of S2S droughts in existing Earth system models. This, in turn, could potentially support the development of drought risk mitigation strategies under future climate. Our contributions are summarized as follows:

- We introduce DroughtSet, a drought prediction dataset for the machine learning community. It serves as a complementary resource to existing climate datasets. DroughtSet is a collection of droughts indices and the corresponding climate, physical, and vegetation conditions, specifically focusing on the contiguous U.S. DroughtSet will be released upon the acceptance of this work.
- To forecast drought, we propose *SPDrought*, a spatial-temporal drought prediction model that incorporates geographic neighbor features fusion. It jointly uses both static and dynamic features to accurately predict three key drought indices.
- We leverage the Integrated Gradient to interpret the hidden relationship between the predicted drought indices and the climate, physical, and vegetation features. The interpretability module offers new insights into the dependence structures of among the drought-related physical and ecological variables in the Earth system.

2 DroughtSet

In this section, we introduce DroughtSet, a collection of climate, physical, vegetation conditions, and drought indices from multiple publicly available remote sensing and reanalysis datasets. We selected these variables based on their relevance and potential influence on the mechanisms of drought initiation and development.

2.1 Data Collection and Preprocessing

DroughtSet includes weekly climate-related data from 2003 to 2013 (11 years, 572 weeks) across CONUS covering an

area of over 8 M km². The details of drought/feature types, variables, and their sources are outlined in Table 1. To ensure consistency in geographical resolution, all variables have been resampled to a 4 km spatial scale. The spatial data are represented as a grid of 585 × 1386 pixels across CONUS, with the values in each pixel denoted as $P(i, j)$, where (i, j) are the spatial coordinates of the pixel on the map. Note that, 42% of this pixel area consists of the ocean that is outside the scope here. Only the remaining 58% pixels are used in the analyses. Furthermore, all temporal variables are aggregated to a weekly time scale, detailed in Section 2.2. For the static variables, both elevation and canopy height are numeric variables while land cover is a categorical variable with 97 categories. We also include the mean and standard deviation of the drought indices as the static variables. In total, the dataset comprises 585 × 1386 × 11 × 52 × 3 Drought indices, 585 × 1386 × 11 × 52 × 11 dynamic predictors, and 585 × 1386 × 9 static predictors. Note that NaN values exist in the datasets due to different temporal coverages of remote sensing-derived products.

2.2 Drought indices and Predictors

DroughtSet focuses on three drought types: soil moisture drought measured by surface soil moisture (SM), ecohydrological drought measured by Evaporative Stress Index (ESI), and ecological drought measured by the solar-induced chlorophyll fluorescence (SIF), all normalized using their quantiles at each location. These drought indices are denoted as $D_{i,j}(t) = [d_{i,j}^1(t), \dots, d_{i,j}^K(t)]$, K is the number of indices, which equals to 3 in this case.

- **Soil Moisture:** Low surface soil moisture reflects soil moisture drought intensity and is key to a wide range of ecosystem functions and drought propagation to other downstream drought types (Yuan et al. 2023).
- **Evaporative Stress Index:** ESI is the ratio between actual evapotranspiration and potential evapotranspiration. Low ESI values represent ecohydrological droughts with low moisture supply from the land relative to the demand of the atmosphere. ESI is affected by plant stomatal response to moisture deficit and regulates drought intensification through atmospheric feedback (Nguyen et al. 2019).
- **Solar-induced chlorophyll Fluorescence:** SIF is a surrogate highly correlated with gross primary productivity. Low SIF values reflect impaired photosynthetic activity, offering an effective representation of ecological droughts given its high sensitivity to water stresses (He et al. 2019).

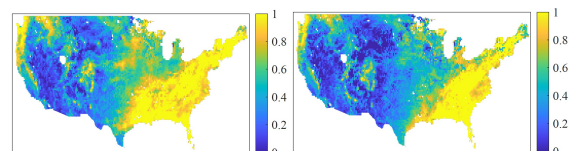


Figure 1: An example of drought development in July 2012. The left and right panels show the evaporative stress index in the 28th and 32nd weeks in 2012, respectively. ESI reduced in the Central Plains, indicating ecohydrological drought.

Table 1: Variables used to quantify three types of droughts and their predictive features.

Drought/Feature Type	Variables	Dynamic or Static	Dataset & Native Resolution
Soil moisture drought	Soil Moisture across depths (SM)	Dynamic	NLDAS (Xia et al. 2012), hourly, 1/8°
Ecohydrological drought	Evaporative stress index (ESI)	Dynamic	ALEXI (Holmes et al. 2018; Liu, Holtzman, and Konings 2021), weekly, 0.25° GridMET (Abatzoglou 2013), daily, 4 km
Ecological drought	Solar-induced fluorescence (SIF)	Dynamic	CSIF (Zhang et al. 2018), 4-day, 0.05°
Physical & climate features	2m temperature, radiation, VPD, precipitation, wind speed, PET, PDSI, SP elevation	Dynamic	GridMET (Abatzoglou 2013), daily, 4 km
		Static	ERA5 (Muñoz-Sabater et al. 2021), hourly, 9 km SRTM (NASA JPL 2013), 30 m
Vegetation features	VOD LAI Canopy Height Land Cover	Dynamic	VODCA (Moesinger et al. 2020), daily, 0.25°
		Dynamic	MODIS (Myneni, Knyazikhin, and Park 2015), 8-day, 500 m
		Static	GLAD (Potapov et al. 2021), 30 m
		Static	NLCD (Homer, Fry, and Barnes 2012; Homer et al. 2020), 30 m

These metrics are of focus here for S2S drought because, unlike other commonly used drought severity indices such as the Standardized Precipitation Index and Palmer Drought Severity Index (PDSI) that are typically used to capture interannual drought, these metrics have been demonstrated to respond quickly and have wide-ranging implications on water resources, ecosystem carbon sink strength, and agricultural productivity (Christian et al. 2021; Ford et al. 2023; He et al. 2019; Koster et al. 2019; Nguyen et al. 2019; Yuan et al. 2023). In our work, these drought indices are used as the targets to be predicted. Figure 1 visualizes the evaporative stress, using the 2012 central US drought as an example, which illustrates the pattern of a drought index.

To predict the three drought indices, we use attributes including climate and physical conditions, ecological conditions, and drought indices themselves in lagged time steps as features for drought prediction. These features are categorized as temporal dynamic attributes and spatial static attributes that will be considered differently in *SPDrought*. These features are described in the following.

Physical and climate conditions:

- **Elevation:** Elevation is a static numeric variable. It affects local climate, subsurface hydrological processes, and thus drought occurrence and intensity.
- **Air Temperature:** Air temperature and the following climate conditions are all dynamic numeric variables. High air temperatures accelerate soil moisture depletion and intensify atmospheric demand, thereby facilitating drought intensification.
- **Precipitation:** It determines the amount of water input to the land. Precipitation deficit directly leads to drought.
- **Radiation:** Incident solar radiation controls the available energy that drives water loss from the land to the atmosphere. High radiation could accelerate water loss rate and thus drought onset.
- **Vapor Pressure Deficit (VPD):** VPD characterizes atmospheric moisture deficit and drives evapotranspiration through aerodynamic processes.

- **Wind Speed:** High wind speed enhances aerodynamic conductance and thus water and heat transfer rates from the land to the atmosphere, thereby potentially contributing to drought initiation development.
- **Potential Evapotranspiration (PET):** PET represents the atmospheric water demand.
- **PDSI:** It quantifies the severity of meteorological drought based on meteorological conditions and an empirical water balance model, which primarily characterizes long-term droughts.
- **Surface Pressure (SP):** SP is the atmospheric pressure at Earth’s surface. Changes in surface pressure can regulate weather patterns, atmospheric moisture transport, and thus drought occurrence.
- **SM Root:** Different from surface soil moisture, root zone soil moisture measures the amount of water available to plant water uptake.

Ecological conditions:

- **Biomass dynamics measured by Leaf Area Index (LAI):** LAI represents the leaf area per ground unit area. We aggregate it from the original 8-day temporal steps to weekly steps using linear interpolation.
- **Vegetation Optical Depth (VOD):** VOD represents total vegetation water content.
- **Canopy Height:** Canopy height is a static categorical variable, representing ecosystem structure.
- **Land Cover:** It is a static categorical variable, including categories such as forests, water bodies, and grasslands.

With these climate-related drought indices and attributes, each pixel has N static features $S_{i,j} = [s_{i,j}^1, \dots, s_{i,j}^N]$ (i.e., land cover, elevation, canopy height, long-term averages of drought indices and their standard deviations to capture variability) and M dynamic features $X_{i,j}(t) = [x_{i,j}^1(t), \dots, x_{i,j}^M(t)]$. The goal is to train a machine learning model $h \in \mathcal{H}$ from existing static and dynamic features $\{S_{i,j}, D_{i,j}(t), X_{i,j}(t)\}_{i \in [I], j \in [J], t \in [T]}$ that can simultaneously predict multiple drought indices $\{D_{i,j}(T + \tau)\}_{\tau \geq 1}$

for any location (i, j) in the future. Because both drought indices $D_{i,j}(t)$ and dynamic features $X_{i,j}(t)$ are time-varying and jointly used for predictive tasks, we combine them and define $U_{i,j}(t) = [D_{i,j}(t), X_{i,j}(t)]$.

In addition, as DroughtSet consists of both static features and temporal features for each location with geographic coordinates, it offers a versatile platform for benchmarking various forecasting methods. This dataset can be utilized in univariate forecasting tasks, which focus on directly predicting drought indices from single variables. It also supports multivariate forecasting, where multiple variables are used jointly to predict drought indices. Furthermore, DroughtSet is ideal for spatiotemporal forecasting, which leverages both spatial and temporal information to enhance prediction accuracy. Lastly, it can be employed in irregular forecasting tasks that jointly use static and temporal features, providing a comprehensive tool for advanced drought prediction models.

3 Method

Next, we introduce a comprehensive framework that utilizes both spatial and temporal information to predict drought indices. Our approach considers regional spatial similarity to aggregate information for robust prediction and introduces climate attribute-specific representation functions to learn from the hidden pattern of both static and time-series data.

Spatial-Temporal Fusion. Since climate information from proximate geographical locations often exhibits mutual influences, we hypothesize that data from neighboring locations may contain useful information that can help enhance the accuracy and reliability of the prediction. The key challenge is to exploit the spatial correlation and strategically leverage the learned correlation to enhance prediction at the target location. Intuitively, the target location may benefit more from those neighbors that are sufficiently correlated, e.g., sharing similar topography or land cover. Let neighborhood $\mathcal{N}_{i,j} = \{(\bar{i}, \bar{j}) \mid (|\bar{i} - i| \leq d, |\bar{j} - j| \leq d, (\bar{i}, \bar{j}) \neq (i, j))\}$, where d is a distance threshold. Inspired by scaled dot-product attention mechanism (Vaswani et al. 2017), we exploit the spatial correlation between any target location (i, j) (known as a query in attention mechanism) and neighbors in $\mathcal{N}_{i,j}$ (known as keys) based on the following:

$$A = \text{softmax} \left(\frac{(S_{i,j} W_{\text{query}})(S_{\mathcal{N}_{i,j}} W_{\text{key}})^T}{R_{i,j} \times \sqrt{N}} \right) \quad (1)$$

where $S_{i,j}$ are N static features at (i, j) , $S_{\mathcal{N}_{i,j}}$ is a matrix with each column the static features corresponding to one neighbor in $\mathcal{N}_{i,j}$. $W_{\text{query}} \in \mathbb{R}^{N \times N}$ and $W_{\text{key}} \in \mathbb{R}^{N \times N}$ are two linear transformation matrices that are learned to exploit spatial correlation. $R_{i,j}$ is a vector with each element the Euclidean distance between (i, j) and neighbors in $\mathcal{N}_{i,j}$, which leverages the prior spatial information to refine correlation learning process. For simplicity, we consider a 5×5 square area in this study, where d is set to 2 in this paper. To avoid division by zero, we manually set the distance to itself as 0.8. The spatial correlation weight A can then be used to aggregate the regional time-varying attributes: $\tilde{U}_{\bar{i}, \bar{j}}(t) = \sum_{\bar{i}, \bar{j} \in \mathcal{N}_{i,j}} A_{\bar{i}, \bar{j}} \cdot U_{\bar{i}, \bar{j}}(t)$.

Spatial-Temporal Representation and Multi-task Learning. Given $\{S_{i,j}, \tilde{U}_{i,j}(t)\}$, we next learn the representations of the climate data, which combine static and dynamic feature representations generated by separated networks:

- **Static feature representation:** Given a set of static features $S_{i,j} = [s_{i,j}^1, \dots, s_{i,j}^N]$, we aim to obtain higher-level representation that encapsulates the underlying patterns among them. Because categorical (land cover type) and numerical (elevation, canopy height, long-term averages, and standard deviations of SM, SIF, and ESI) features have inherent differences in semantic meanings, we shall generate their representations differently. We apply two layers of MLP linked by the ReLU function to learn the representations of numerical features and adopt embedding approaches for categorical features to generate their representations, which we denote as $f_{i,j}^s$.
- **Dynamic feature representation:** To learn the temporal patterns, especially the long-term dependencies of climate data, we first adapt *Transformer* (Vaswani et al. 2017) encoder to generate temporal representations. Before the *Transformer*, we expand the initial temporal features $\tilde{U}_{i,j}(t)$ of our data (including K drought indices and M dynamic features with a total dimension of 14) via linear transformation W and project the dimensions to 48. This linear transformation also facilitates learning the interconnections among these distinct dynamic features. After integrating the *positional encoding* $\text{PE}(t)$, we generate temporal representation $f_{i,j}^t(t) = \text{TransformerEncoder}(\tilde{U}_{i,j}(t) \cdot W + \text{PE}(t))$. We then concatenate the static representations to dynamic feature representations at each time stamp. The concatenated representations are fed into the *Transformer decoder* to generate representations $\{F_{i,j}(t')\}_{t' \in \{T+1 \dots T+26\}}$ for the next 26 weeks.

With the representation $\{F_{i,j}(t')\}_{t' \in \{T+1 \dots T+26\}}$ for the prediction weeks, we employ three *task-specific* regressors to map the representation of the next 26 weeks to drought indices. Specifically, let $\hat{d}_{i,j}^k(t') = \text{Regressor}_k(F_{i,j}(t'))$ be the prediction of k -th drought index $d_{i,j}^k(t')$ after t' weeks. We jointly train all the parameters by minimizing the total loss between predictions $\hat{d}_{i,j}^k(t')$ and ground-truth $d_{i,j}^k(t')$ for all drought indices at all locations (we use a batch of locations to update the model at every iteration in implementation) under mean absolute error loss function \mathcal{L} :

$$\min \sum_{k \in [K]} \sum_{t' \in \{T+1 \dots T+26\}} \sum_{i \in [I], j \in [J]} \mathcal{L}(\hat{d}_{i,j}^k(t'), d_{i,j}^k(t')). \quad (2)$$

Interpreting the impacts of attributes on drought. To identify which attributes and time steps contribute most to the final predictions, we leverage integrated gradient (Sundararajan, Taly, and Yan 2017) to investigate how their contributions to the final predictions change over time (i.e., how *sensitive* the predictions are to these features). The integrated gradient estimates feature sensitivities by integrating the gradients of the model’s output with respect to the input along a straight path from an “input baseline” to the input. Then we quantify

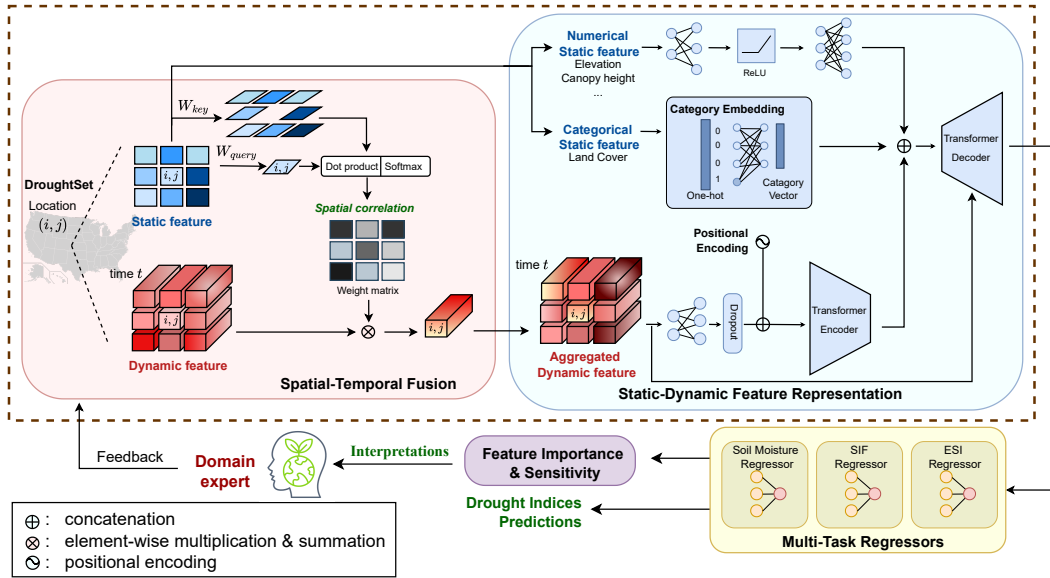


Figure 2: *SPDrought* architecture for Forecasting Drought Indices: the spatial-temporal fusion module first exploits the spatial correlation of data with its neighbors using static features and leverages the learned correlation to aggregate the dynamic features; the static-dynamic feature representation exploits both spatial and temporal patterns with three network modules. Such representation is shared among multi-task regressors for generating multiple drought indices predictions. Subsequently, we analyze how individual features at various timestamps influence the final predictions using our interpretation method. Domain experts are encouraged to provide feedback on variable selection and model design, which can further refine the model and uncover deeper relationships among variables.

the importance of static variables by looking at the features that cause the larger performance change and are more important for prediction tasks.

4 Experiments

4.1 Experimental setup

Training details. All experiments are conducted on a server equipped with multiple NVIDIA V100 GPUs, Intel Xeon(R) Platinum 8260 CPU, and 256GB memory. The code is implemented with Python 3.9 and PyTorch 1.10.0.

In this study, we split the pixels by 5×5 pixel block to avoid similar neighboring pixels and randomly select 80% blocks as training pixels and the remaining 20% for testing. Each pixel in our dataset has 572 weeks of temporal features and drought indices. We divide these 572 weeks into multiple windows for training and analysis. Each window consists of 100 weeks (approximately 2 years) designated as the training period, followed by 26 weeks (approximately half a year) designated as the prediction period. We then slide this window forward by 26 weeks (half a year) at a time, creating a total of 18 overlapping windows. To mitigate the impact of missing values (NaN) in the dataset, we impute the yearly average value for each week to maintain seasonal trends. Training is skipped for any NaN values in drought indices. Additionally, before training, we normalize each predictor and drought index by dividing it by its maximum value, scaling all values to a range between 0 and 1.

During the training, we sample a batch of pixels randomly

and shuffle the order of these windows to sequentially update the model. We train the model over 30 epochs where an epoch is defined as each training pixel being visited and trained once. After filtering out ocean locations, where most variables are NaN, the number of effective training pixels totals 380,801. The test set comprises 93,220 effective pixels. We set the batch size to 32, and employ Adam optimizer with a learning rate of $1e-4$. The mean absolute error is used as the loss function. For categorical variable land cover, the embedding dimension is set at 4. For static numeric variables, the MLP uses a hidden dimension of 10 and an output dimension of 16. Temporal features are first processed through a linear layer with a dropout rate of 0.1, mapping the dimension from 14 to 48. Then three layers of Transformer encoders and two layers of decoders with dimensions of 256 and 2 attention heads are used to learn from the projected temporal features. The model has 1M trainable parameters. Training on the entire training set takes approximately 80 minutes per epoch, and inference on the test set takes around 5 minutes.

Baselines. We consider state-of-the-art deep learning methods for time-series forecasting as baselines to evaluate our method. Note that these methods are mostly designed for time-series features without considering static features, including Transformer (Vaswani et al. 2017), Informer (Zhou et al. 2021), PatchTST (Nie et al. 2023), DLinear (Zeng et al. 2023), iTransformer (Liu et al. 2023), TimesNet (Wu et al. 2022a), and LSTM (Hochreiter and Schmidhuber 1997). We introduce the details of each baseline in Appendix 6.1.

Table 2: Average mean absolute error over three experiments (standard deviations are reported in the appendix).

MAE ($\times 10^{-3}$)	SPDrought	Transformer	Informer	PatchTST	DLinear	iTransformer	TimesNet	LSTM
Soil Moisture	21.39	34.56	38.08	36.32	47.61	32.34	25.96	31.36
ESI	4.40	5.99	6.37	6.37	6.82	6.06	5.11	5.83
SIF	12.21	16.00	17.71	21.36	20.99	15.47	14.11	15.35
Total	38.01	56.56	62.16	64.05	75.41	53.87	45.18	52.54

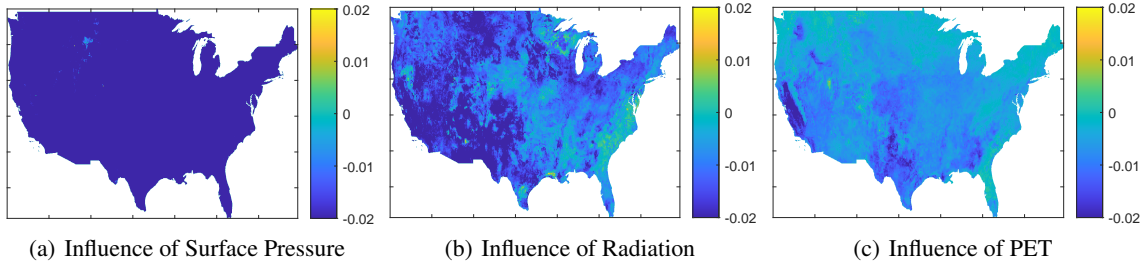


Figure 3: The sensitivity of soil moisture to the top three predictive features measured by the integrated gradient, including surface pressure, radiation, and PET.

4.2 Results

Performance Comparison. We first compare *SPDrought* with five widely recognized time-series forecasting baseline models. Table 2 presents the average mean absolute error across three runs on DroughtSet. The results demonstrate that *SPDrought* has superior forecasting performance at forecasting 26 weeks of three drought indices at test locations compared with baselines. This outcome underscores its effectiveness in capturing the dynamics of the variables under study—Soil Moisture, Evaporative Stress Index, and Solar-induced Chlorophyll Fluorescence.

Among the baselines, *DLinear* has previously shown robust performance, outperforming several transformer-based methods (Zeng et al. 2023) in forecasting. *DLinear* decomposes the time series and uses two linear layers for trend and abnormality respectively. However, *DLinear* encounters challenges with drought indices forecasting tasks because it uses prediction variables (drought indices) independently rather than leveraging all predictors and indices together. In contrast, transformer-based methods typically account for patterns among variables, resulting in better performance in our tasks. It highlights the importance of learning the interplay of predictors to improve forecasting performance in drought prediction challenges. We also compare our model with a vanilla *Transformer*. Except for the main difference in using static features, the *Transformer* baseline uses embedding for temporal input tokenization as same as other methods, while our model considers the linear transformation for the temporal features to learn the representation across predictors.

Drought Interpretation. To examine the relative contribution of features to drought, we study the S2S drought in July 2012 in the CONUS. Specifically, we evaluate the influence of each variable on soil moisture prediction by comparing the integrated gradient value in Figure 3. We select and present the top 3 variables showing their spatial patterns of the largest lag-1 integrated gradient during a drought week. Surface pres-

sure, radiation, and PET show strong negative contributions (negative gradients) to soil moisture. That is, higher values of these metrics lead to decreases in soil moisture, thus potentially contributing to drought. Mechanistically, a higher surface pressure typically leads to drier weather by reducing the likelihood of rainfall, which in turn leads to drier soil conditions. In contrast, low-pressure systems are often associated with increased cloud cover and precipitation, which tend to enhance soil moisture (Bonan 2019). Additionally, both high solar radiation and high PET could enhance evapotranspiration, thus reducing soil moisture. Thus, the data-driven integrated gradient is able to recover the mechanistic dependency of soil moisture on climate conditions. Figure 4 shows the top 3 predictors influencing the Evaporative Stress Index, i.e., radiation, surface pressure, and SIF, where higher levels of surface pressure contribute to increased evaporative stress index. Figure 5 shows pressure, radiation, and root zone soil moisture largely influence SIF. In particular, low radiation and low root zone moisture would reduce SIF, contributing to ecological drought. The impacts are especially apparent in the eastern US where vegetation is relatively denser compared to the western US. These observed results are consistent with first-order hydrological and ecological principles. The results on interoperability reveal the relative importance of these predictors to each drought index. The relative magnitudes and their spatial patterns contribute to discipline-specific understanding of the development and propagation of droughts.

Assessment of Drought Using Soil Moisture Percentiles.

In this section, we use soil moisture as an example to assess drought by employing a percentile-based approach (Wang and Yuan 2018). Each data point of weekly soil moisture is compared against a multi-year average for the same calendar week, derived from historical data to represent typical moisture levels. We calculate the deviation of current soil moisture levels from these averages. We then use the 30th percentile as the threshold in our analysis. Soil moisture values below this percentile are considered as soil moisture drought. *SP-*

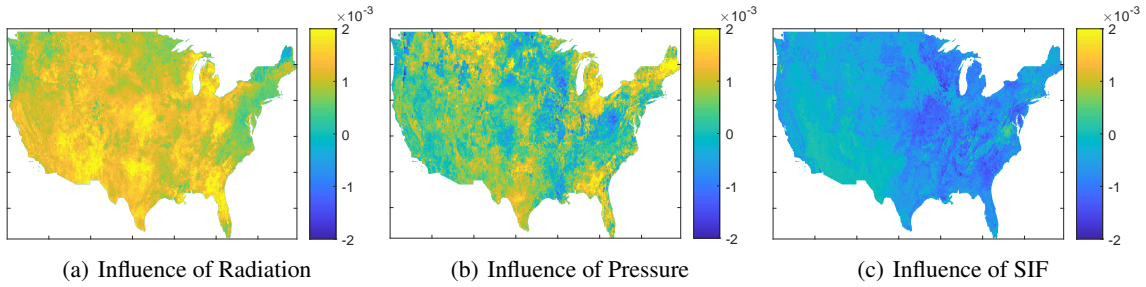


Figure 4: The sensitivity of Evaporative Stress Index. Radiation and Pressure show a positive influence on the evaporative stress index while SIF reflects a minor negative influence.

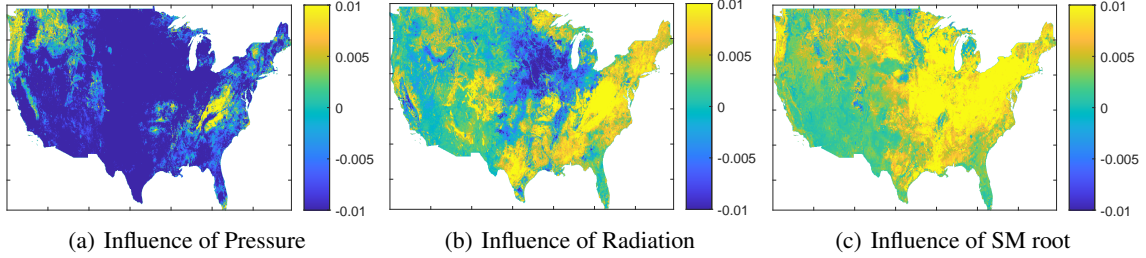
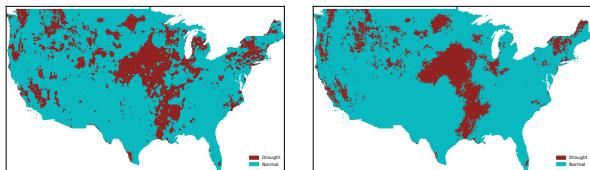


Figure 5: The sensitivity of Solar-induced Fluorescence. Both radiation and root-zone soil moisture directly influence the rate of photosynthesis, which in turn affects the SIF signal.

Table 3: Evaluation of drought prediction by soil moisture. The standard deviations are reported in the Appendix.

	SPDrought	Transformer	Informer	PatchTST	DLinear	iTransformer	TimesNet	LSTM
Accuracy	86.26	76.09	72.16	62.24	62.85	77.18	81.54	77.45
Precision	76.80	59.94	53.40	36.94	37.96	61.74	68.98	62.18

Drought is compared with other methods in terms of accuracy and precision. Results on the test set are reported in Table 3.



(a) Soil moisture drought detected from reanalysis data (b) Soil moisture drought based on the prediction

Figure 6: Comparison of observation-based soil moisture drought and that predicted using our model *SPDrought* with a lead time of 6 weeks in July 2012.

We visualize the predicted soil moisture drought in July 2012. Figure 6.a. shows the observation-based soil moisture drought derived from the reanalysis product. For comparison, Figure 6.b shows the drought derived from the soil moisture predicted using *SPDrought*. The results show that *SPDrought* successfully predicts the spatial pattern of observed soil moisture drought, especially in the Central Plains. In addition, we conduct ablation studies on static variables and model components, which are reported in Appendix 6.3.

5 Conclusion

This paper introduces DroughtSet, a specialized time-series forecasting dataset for predicting drought indices. It integrates vegetation and climate predictors that include both static and dynamic features. Based on DroughtSet, we propose *SPDrought*, which exploits spatial-temporal interactions among the features to predict drought indices while providing interpretations on the impacts of each predictor on drought indices. Our findings contribute to improved understanding and prediction of drought development and propagation.

Limitation and Future Work. This paper focuses on CONUS as a case study. Therefore, the trained model on DroughtSet is not suitable for direct deployment in other regions because of geographical differences. However, our method is not limited to CONUS and is expected to be effective in other regions, provided that relevant remote sensing and reanalysis datasets are available at a global scale. We suggest that expert knowledge is still needed to interpret the physical processes with complex mechanisms, such as the drivers of evaporative stress. In this study, we primarily examine the spatial influence of physical and climate conditions and vegetation dynamics on drought indices. Future case studies could benefit from comprehensive analyses of the temporal interplay among dynamic predictors and the dependencies related to S2S droughts.

Acknowledgements

This material is based upon work supported by the U.S. National Science Foundation under award IIS-2202699 and IIS-2416895, by OSU President's Research Excellence Accelerator Grant, and grants from the Ohio State University's Translational Data Analytics Institute and College of Engineering Strategic Research Initiative.

References

- Abatzoglou, J. T. 2013. Development of gridded surface meteorological data for ecological applications and modelling. *International journal of climatology*, 33(1): 121–131.
- Adede, C.; Oboko, R.; Wagacha, P. W.; and Atzberger, C. 2019. A mixed model approach to vegetation condition prediction using artificial neural networks (ANN): case of Kenya's operational drought monitoring. *Remote Sensing*, 11(9): 1099.
- Agana, N. A.; and Homaifar, A. 2017. A deep learning based approach for long-term drought prediction. In *SoutheastCon 2017*, 1–8. IEEE.
- AghaKouchak, A.; Pan, B.; Mazdiyasn, O.; Sadegh, M.; Jiwa, S.; Zhang, W.; Love, C.; Madadgar, S.; Papalexiou, S.; Davis, S.; et al. 2022. Status and prospects for drought forecasting: Opportunities in artificial intelligence and hybrid physical–statistical forecasting. *Philosophical Transactions of the Royal Society A*, 380(2238): 20210288.
- Amanambu, A. C.; Mossa, J.; and Chen, Y.-H. 2022. Hydrological drought forecasting using a deep transformer model. *Water*, 14(22): 3611.
- Bonaccorso, B.; Cancelliere, A.; and Rossi, G. 2015. Probabilistic forecasting of drought class transitions in Sicily (Italy) using standardized precipitation index and North Atlantic oscillation index. *Journal of Hydrology*, 526: 136–150.
- Bonan, G. 2019. *Climate change and terrestrial ecosystem modeling*. Cambridge University Press.
- Christian, J. I.; Basara, J. B.; Hunt, E. D.; Otkin, J. A.; Furtado, J. C.; Mishra, V.; Xiao, X.; and Randall, R. M. 2021. Global distribution, trends, and drivers of flash drought occurrence. *Nature communications*, 12(1): 6330.
- Cook, B. I.; Mankin, J. S.; and Anchukaitis, K. J. 2018. Climate change and drought: From past to future. *Current Climate Change Reports*, 4: 164–179.
- Danandeh Mehr, A.; Rikhtehgar Ghiasi, A.; Yaseen, Z. M.; Sorman, A. U.; and Abualigah, L. 2023. A novel intelligent deep learning predictive model for meteorological drought forecasting. *Journal of Ambient Intelligence and Humanized Computing*, 14(8): 10441–10455.
- Das, N. N.; Entekhabi, D.; Dunbar, R. S.; Colliander, A.; Chen, F.; Crow, W.; Jackson, T. J.; Berg, A.; Bosch, D. D.; Caldwell, T.; et al. 2018. The SMAP mission combined active-passive soil moisture product at 9 km and 3 km spatial resolutions. *Remote sensing of environment*, 211: 204–217.
- Dikshit, A.; and Pradhan, B. 2021. Interpretable and explainable AI (XAI) model for spatial drought prediction. *Science of the Total Environment*, 801: 149797.
- Dikshit, A.; Pradhan, B.; and Alamri, A. M. 2021. Long lead time drought forecasting using lagged climate variables and a stacked long short-term memory model. *Science of The Total Environment*, 755: 142638.
- Ferchichi, A.; Abbes, A. B.; Barra, V.; and Farah, I. R. 2022. Forecasting vegetation indices from spatio-temporal remotely sensed data using deep learning-based approaches: A systematic literature review. *Ecological Informatics*, 68: 101552.
- Ford, T. W.; Otkin, J. A.; Quiring, S. M.; Lisonbee, J.; Woloszyn, M.; Wang, J.; and Zhong, Y. 2023. Flash Drought Indicator Intercomparison in the United States. *Journal of Applied Meteorology and Climatology*, 62(12): 1713–1730.
- Gyaneshwar, A.; Mishra, A.; Chadha, U.; Raj Vincent, P. D.; Rajinikanth, V.; Pattukandan Ganapathy, G.; and Srinivasan, K. 2023. A contemporary review on deep learning models for drought prediction. *Sustainability*, 15(7): 6160.
- Ham, Y.-G.; Kim, J.-H.; and Luo, J.-J. 2019. Deep learning for multi-year ENSO forecasts. *Nature*, 573(7775): 568–572.
- Hao, Z.; Singh, V. P.; and Xia, Y. 2018. Seasonal drought prediction: Advances, challenges, and future prospects. *Reviews of Geophysics*, 56(1): 108–141.
- He, M.; Kimball, J. S.; Yi, Y.; Running, S.; Guan, K.; Jencso, K.; Maxwell, B.; and Maneta, M. 2019. Impacts of the 2017 flash drought in the US Northern plains informed by satellite-based evapotranspiration and solar-induced fluorescence. *Environmental Research Letters*, 14(7): 074019.
- Hochreiter, S.; and Schmidhuber, J. 1997. Long short-term memory. *Neural computation*, 9(8): 1735–1780.
- Holmes, T. R.; Hain, C. R.; Crow, W. T.; Anderson, M. C.; and Kustas, W. P. 2018. Microwave implementation of two-source energy balance approach for estimating evapotranspiration. *Hydrology and earth system sciences*, 22(2): 1351–1369.
- Homer, C.; Dewitz, J.; Jin, S.; Xian, G.; Costello, C.; Danielson, P.; Gass, L.; Funk, M.; Wickham, J.; Stehman, S.; et al. 2020. Conterminous United States land cover change patterns 2001–2016 from the 2016 national land cover database. *ISPRS Journal of Photogrammetry and Remote Sensing*, 162: 184–199.
- Homer, C. G.; Fry, J. A.; and Barnes, C. A. 2012. The national land cover database. Technical report, US Geological Survey.
- Jiang, J.; Han, C.; Zhao, W. X.; and Wang, J. 2023. Pdformer: Propagation delay-aware dynamic long-range transformer for traffic flow prediction. In *Proceedings of the AAAI conference on artificial intelligence*, volume 37, 4365–4373.
- Kaur, A.; and Sood, S. K. 2020. Deep learning based drought assessment and prediction framework. *Ecological Informatics*, 57: 101067.
- Kaushik, S.; Choudhury, A.; Sheron, P. K.; Dasgupta, N.; Natarajan, S.; Pickett, L. A.; and Dutt, V. 2020. AI in healthcare: time-series forecasting using statistical, neural, and ensemble architectures. *Frontiers in big data*, 3: 4.
- Khan, M. I.; and Maity, R. 2024. Development of a Long-Range Hydrological Drought Prediction Framework Using Deep Learning. *Water Resources Management*, 38(4): 1497–1509.

- Khan, N.; Sachindra, D.; Shahid, S.; Ahmed, K.; Shiru, M. S.; and Nawaz, N. 2020. Prediction of droughts over Pakistan using machine learning algorithms. *Advances in Water Resources*, 139: 103562.
- Koster, R.; Schubert, S.; Wang, H.; Mahanama, S.; and DeAngelis, A. M. 2019. Flash drought as captured by reanalysis data: Disentangling the contributions of precipitation deficit and excess evapotranspiration. *Journal of Hydrometeorology*, 20(6): 1241–1258.
- Lees, T.; Tseng, G.; Atzberger, C.; Reece, S.; and Dadson, S. 2022. Deep learning for vegetation health forecasting: a case study in Kenya. *Remote Sensing*, 14(3): 698.
- Liang, Y.; Xia, Y.; Ke, S.; Wang, Y.; Wen, Q.; Zhang, J.; Zheng, Y.; and Zimmermann, R. 2023. Airformer: Predicting nationwide air quality in china with transformers. In *Proceedings of the AAAI Conference on Artificial Intelligence*, volume 37, 14329–14337.
- Liu, Y.; Holtzman, N. M.; and Konings, A. G. 2021. Global ecosystem-scale plant hydraulic traits retrieved using model–data fusion. *Hydrology and Earth System Sciences*, 25(5): 2399–2417.
- Liu, Y.; Hu, T.; Zhang, H.; Wu, H.; Wang, S.; Ma, L.; and Long, M. 2023. iTransformer: Inverted Transformers Are Effective for Time Series Forecasting. In *The Twelfth International Conference on Learning Representations*.
- Marj, A. F.; and Meijerink, A. M. 2011. Agricultural drought forecasting using satellite images, climate indices and artificial neural network. *International Journal of Remote Sensing*, 32(24): 9707–9719.
- Mo, K. C.; and Lettenmaier, D. P. 2020. Prediction of flash droughts over the United States. *Journal of Hydrometeorology*, 21(8): 1793–1810.
- Moesinger, L.; Dorigo, W.; De Jeu, R.; Van Der Schalie, R.; Scanlon, T.; Teubner, I.; and Forkel, M. 2020. The global long-term microwave vegetation optical depth climate archive (VODCA). *Earth System Science Data*, 12(1): 177–196.
- Mohammadi, K.; Jiang, Y.; and Wang, G. 2022. Flash drought early warning based on the trajectory of solar-induced chlorophyll fluorescence. *Proceedings of the National Academy of Sciences*, 119(32): e2202767119.
- Mouatadid, S.; Orenstein, P.; Flaspohler, G.; Cohen, J.; Opreescu, M.; Fraenkel, E.; and Mackey, L. 2023. Adaptive bias correction for improved subseasonal forecasting. *Nature Communications*, 14(1): 3482.
- Muñoz-Sabater, J.; Dutra, E.; Agustí-Panareda, A.; Albergel, C.; Arduini, G.; Balsamo, G.; Boussetta, S.; Choulga, M.; Harrigan, S.; Hersbach, H.; et al. 2021. ERA5-Land: A state-of-the-art global reanalysis dataset for land applications. *Earth system science data*, 13(9): 4349–4383.
- Myneni, R.; Knyazikhin, Y.; and Park, T. 2015. MCD15A3H MODIS/Terra+ Aqua Leaf Area Index/FPAR 4-day L4 Global 500 m SIN Grid V006, NASA EOSDIS Land Processes DAAC [data set].
- NASA JPL. 2013. NASA Shuttle Radar Topography Mission Global 1 arc second. <https://doi.org/10.5067/MEaSURES/SRTM/SRTMGL1.003>. Accessed 2024-05-17.
- Nguyen, H.; Wheeler, M. C.; Otkin, J. A.; Cowan, T.; Frost, A.; and Stone, R. 2019. Using the evaporative stress index to monitor flash drought in Australia. *Environmental Research Letters*, 14(6): 064016.
- Nguyen, T.; Brandstetter, J.; Kapoor, A.; Gupta, J. K.; and Grover, A. 2023. ClimaX: A foundation model for weather and climate. In *International Conference on Machine Learning*, 25904–25938. PMLR.
- Nie, Y.; H. Nguyen, N.; Sinthong, P.; and Kalagnanam, J. 2023. A Time Series is Worth 64 Words: Long-term Forecasting with Transformers. In *International Conference on Learning Representations*.
- Otkin, J. A.; Anderson, M. C.; Hain, C.; and Svoboda, M. 2014. Examining the relationship between drought development and rapid changes in the evaporative stress index. *Journal of Hydrometeorology*, 15(3): 938–956.
- Otkin, J. A.; Svoboda, M.; Hunt, E. D.; Ford, T. W.; Anderson, M. C.; Hain, C.; and Basara, J. B. 2018. Flash droughts: A review and assessment of the challenges imposed by rapid-onset droughts in the United States. *Bulletin of the American Meteorological Society*, 99(5): 911–919.
- Park, S.; Singh, K.; Nellikkattil, A.; Zeller, E.; Mai, T. D.; and Cha, M. 2022. Downscaling earth system models with deep learning. In *Proceedings of the 28th ACM SIGKDD conference on knowledge discovery and data mining*, 3733–3742.
- Park, Y.-J.; Seo, M.; Kim, D.; Kim, H.; Choi, S.; Choi, B.; Ryu, J.; Son, S.; Jeon, H.-G.; and Choi, Y. 2023. Long-Term Typhoon Trajectory Prediction: A Physics-Conditioned Approach Without Reanalysis Data. In *The Twelfth International Conference on Learning Representations*.
- Pendergrass, A. G.; Meehl, G. A.; Pulwarty, R.; Hobbins, M.; Hoell, A.; AghaKouchak, A.; Bonfils, C. J.; Gallant, A. J.; Hoerling, M.; Hoffmann, D.; et al. 2020. Flash droughts present a new challenge for subseasonal-to-seasonal prediction. *Nature Climate Change*, 10(3): 191–199.
- Potapov, P.; Li, X.; Hernandez-Serna, A.; Tyukavina, A.; Hansen, M. C.; Kommareddy, A.; Pickens, A.; Turubanova, S.; Tang, H.; Silva, C. E.; et al. 2021. Mapping global forest canopy height through integration of GEDI and Landsat data. *Remote Sensing of Environment*, 253: 112165.
- Proadhan, F. A.; Zhang, J.; Yao, F.; Shi, L.; Pangali Sharma, T. P.; Zhang, D.; Cao, D.; Zheng, M.; Ahmed, N.; and Mohana, H. P. 2021. Deep learning for monitoring agricultural drought in South Asia using remote sensing data. *Remote Sensing*, 13(9): 1715.
- Santos, J. F.; Portela, M. M.; and Pulido-Calvo, I. 2014. Spring drought prediction based on winter NAO and global SST in Portugal. *Hydrological Processes*, 28(3): 1009–1024.
- Sundararajan, M.; Taly, A.; and Yan, Q. 2017. Axiomatic attribution for deep networks. In *International conference on machine learning*, 3319–3328. PMLR.
- Trenberth, K. E.; Dai, A.; Van Der Schrier, G.; Jones, P. D.; Barichivich, J.; Briffa, K. R.; and Sheffield, J. 2014. Global warming and changes in drought. *Nature Climate Change*, 4(1): 17–22.

- Tripathy, K. P.; Mukherjee, S.; Mishra, A. K.; Mann, M. E.; and Williams, A. P. 2023. Climate change will accelerate the high-end risk of compound drought and heatwave events. *Proceedings of the National Academy of Sciences*, 120(28): e2219825120.
- Vaswani, A.; Shazeer, N.; Parmar, N.; Uszkoreit, J.; Jones, L.; Gomez, A. N.; Kaiser, L.; and Polosukhin, I. 2017. Attention is all you need. *Advances in neural information processing systems*, 30.
- Vo, T. Q.; Kim, S.-H.; Nguyen, D. H.; and Bae, D.-H. 2023. LSTM-CM: a hybrid approach for natural drought prediction based on deep learning and climate models. *Stochastic Environmental Research and Risk Assessment*, 37(6): 2035–2051.
- Wanders, N.; and Wada, Y. 2015. Decadal predictability of river discharge with climate oscillations over the 20th and early 21st century. *Geophysical Research Letters*, 42(24): 10–689.
- Wanders, N.; and Wood, E. F. 2016. Improved sub-seasonal meteorological forecast skill using weighted multi-model ensemble simulations. *Environmental Research Letters*, 11(9): 094007.
- Wang, A.; Bohn, T. J.; Mahanama, S. P.; Koster, R. D.; and Lettenmaier, D. P. 2009. Multimodel ensemble reconstruction of drought over the continental United States. *Journal of Climate*, 22(10): 2694–2712.
- Wang, L.; and Yuan, X. 2018. Two types of flash drought and their connections with seasonal drought. *Advances in Atmospheric Sciences*, 35(12): 1478–1490.
- White, C. J.; Carlsen, H.; Robertson, A. W.; Klein, R. J.; Lazo, J. K.; Kumar, A.; Vitart, F.; Coughlan de Perez, E.; Ray, A. J.; Murray, V.; et al. 2017. Potential applications of subseasonal-to-seasonal (S2S) predictions. *Meteorological applications*, 24(3): 315–325.
- White, C. J.; Domeisen, D. I.; Acharya, N.; Adefisan, E. A.; Anderson, M. L.; Aura, S.; Balogun, A. A.; Bertram, D.; Bluhm, S.; Brayshaw, D. J.; et al. 2022. Advances in the application and utility of subseasonal-to-seasonal predictions. *Bulletin of the American Meteorological Society*, 103(6): E1448–E1472.
- Wu, H.; Hu, T.; Liu, Y.; Zhou, H.; Wang, J.; and Long, M. 2022a. Timesnet: Temporal 2d-variation modeling for general time series analysis. In *The eleventh international conference on learning representations*.
- Wu, H.; Xu, J.; Wang, J.; and Long, M. 2021. Autoformer: Decomposition transformers with auto-correlation for long-term series forecasting. *Advances in neural information processing systems*, 34: 22419–22430.
- Wu, Z.; Yin, H.; He, H.; and Li, Y. 2022b. Dynamic-LSTM hybrid models to improve seasonal drought predictions over China. *Journal of Hydrology*, 615: 128706.
- Xia, Y.; Mitchell, K.; Ek, M.; Sheffield, J.; Cosgrove, B.; Wood, E.; Luo, L.; Alonge, C.; Wei, H.; Meng, J.; et al. 2012. Continental-scale water and energy flux analysis and validation for the North American Land Data Assimilation System project phase 2 (NLDAS-2): 1. Intercomparison and application of model products. *Journal of Geophysical Research: Atmospheres*, 117(D3).
- Yu, W.; Li, J.; Liu, Q.; Zhao, J.; Dong, Y.; Wang, C.; Lin, S.; Zhu, X.; and Zhang, H. 2021. Spatial-temporal prediction of vegetation index with deep recurrent neural networks. *IEEE Geoscience and Remote Sensing Letters*, 19: 1–5.
- Yuan, X.; Wang, Y.; Ji, P.; Wu, P.; Sheffield, J.; and Otkin, J. A. 2023. A global transition to flash droughts under climate change. *Science*, 380(6641): 187–191.
- Zeng, A.; Chen, M.; Zhang, L.; and Xu, Q. 2023. Are transformers effective for time series forecasting? In *Proceedings of the AAAI conference on artificial intelligence*, volume 37, 11121–11128.
- Zhang, L.; Kim, T.; Yang, T.; Hong, Y.; and Zhu, Q. 2021. Evaluation of Subseasonal-to-Seasonal (S2S) precipitation forecast from the North American Multi-Model ensemble phase II (NMME-2) over the contiguous US. *Journal of Hydrology*, 603: 127058.
- Zhang, Y.; Joiner, J.; Alemohammad, S. H.; Zhou, S.; and Gentine, P. 2018. A global spatially contiguous solar-induced fluorescence (CSIF) dataset using neural networks. *Biogeosciences*, 15(19): 5779–5800.
- Zhou, H.; Zhang, S.; Peng, J.; Zhang, S.; Li, J.; Xiong, H.; and Zhang, W. 2021. Informer: Beyond efficient transformer for long sequence time-series forecasting. In *Proceedings of the AAAI conference on artificial intelligence*, volume 35, 11106–11115.
- Zhou, T.; Ma, Z.; Wen, Q.; Wang, X.; Sun, L.; and Jin, R. 2022. Fedformer: Frequency enhanced decomposed transformer for long-term series forecasting. In *International conference on machine learning*, 27268–27286. PMLR.

6 Appendix

6.1 Baselines

We ensured consistent representation dimensions and batch sizes across all baseline methods and adjusted model layers to maintain comparable training times. Additionally, other method-specific hyperparameters are adjusted to improve performance and ensure similar training times across all methods.

- Transformer (Vaswani et al. 2017): A vanilla Transformer for the time-series forecasting task.
- Informer (Zhou et al. 2021): Informer introduces the ProbSparse self-attention mechanism for efficiently capturing long-range dependencies in time series forecasting.
- PatchTST (Nie et al. 2023): PatchTST applies patching techniques to time series data, enhancing the transformer architecture’s performance in capturing temporal patterns.
- DLinear (Zeng et al. 2023): DLinear is a simplified linear model which succeeds many transformer-based models.
- iTransformer (Liu et al. 2023): iTransformer inverted the duties of the self-attention mechanism and the feed-forward network to achieve better performance.
- TimesNet (Wu et al. 2022a): TimesNet considers intraperiod and interperiod variations in 2D space for time series analysis.
- LSTM (Hochreiter and Schmidhuber 1997): LSTM is widely used in drought prediction. We follow the same architecture as existing studies (Yu et al. 2021; Danandeh Mehr et al. 2023; Khan and Maity 2024), with a convolution neural network as the feature extractor and an LSTM network to forecast drought indices.

We use the same representation dimensions and batch size for all baselines. To ensure comparable training times across different methods, we utilize a 3-layer encoder and 2-layer decoder for Transformer, PatchTST, and iTransformer, aligning with our approach. For TimesNet, we employ a 2-layer encoder and 1-layer decoder to maintain training durations similar to those of other baselines.

6.2 Related Work

AI in Climate AI in climate science has received significant attention in recent years. These advancements have enabled researchers to enhance climate models, improve climate prediction accuracy, and gain insights into the dynamics of the Earth system. As examples, AI has been applied to predict El Niño-Southern Oscillation (ENSO) (Ham, Kim, and Luo 2019), Typhoon detection (Park et al. 2023), and climate data downscaling (Park et al. 2022).

Traditional climate models rely on process-based representations and numerical methods to simulate climate and land surface processes, which can be computationally intensive and limited by the resolution and accuracy of climate forcing data. In contrast, deep learning models excel in recognizing complex patterns in large datasets, offering a complementary approach to process-based methods. In particular, some deep

learning models show strong performance in processing temporal features. For example, (Park et al. 2023) successfully used a transformer model to predict typhoon trajectories without relying on reanalysis data. (Liang et al. 2023) proposed AirFormer for nationwide air quality prediction in China. (Nguyen et al. 2023) proposed a foundation model to forecast key climate variables. These examples underscore the growing efficacy and application of machine learning in climate science.

Drought Prediction Drought prediction is one of the important tasks in climate science. Traditional climate models for drought prediction, which rely on process-based models and historical data, often struggle with the chaotic nature of climate systems. For example, the current generation of Earth system models (ESMs) has large biases in predicting precipitation at a sub-seasonal scale and thus flash drought (Zhang et al. 2021; Mouatadid et al. 2023). The Global Ensemble Forecast System based on process-based models, which holds the potential to implement operationally flash drought forecast guidance, also exhibits large prediction errors (Mo and Lettenmaier 2020). Thus, many studies have highlighted the effectiveness of data-driven models in predicting droughts and identifying their key indicators. With the ability to deal with multicollinearity and non-linear relations among predictive features, machine learning (ML) models were applied to predict flash drought from weeks to months, measured by hydrological, meteorological, and agricultural metrics. These methods include support vector machines, random forests, decision trees, etc. For example, Adede et al. (2019) predicts vegetation condition index using a simple ANN model. It is also applied for agricultural drought prediction using satellite images and climate indices Marj and Meijerink (2011). However, these models were built using traditional ML approaches and often require handcrafted feature engineering or cannot effectively learn the feature from the data. As a result, they cannot exploit complex intercorrelation among different features and usually show limited predictive power. To tackle this challenge, recent studies have leveraged more advanced deep learning methods for flash drought predictions, which can learn hierarchical feature representations automatically from data and often outperform traditional ML methods (Ferchichi et al. 2022; Gyaneshwar et al. 2023). For example, deep neural networks have been applied in drought prediction (Agana and Homaifar 2017; Proadhan et al. 2021; Kaur and Sood 2020). Models specifically designed for time-series data, such as LSTM, have also been used for predicting natural drought index (Vo et al. 2023), and agricultural drought conditions (Lees et al. 2022). Dikshit and Pradhan (2021) further combine LSTM with the convolution neural network to predict the meteorological drought index in Eastern Australia and use SHapley Additive exPlanations to understand model outputs. Similar CNN-LSTM combined models are also used in Yu et al. (2021), Danandeh Mehr et al. (2023) and Khan and Maity (2024), where Yu et al. (2021) predicts vegetation Index, Danandeh Mehr et al. (2023) consider meteorological drought forecasting and Khan and Maity (2024) focus on predicting hydrological drought. Amanambu, Mossa, and Chen (2022) further adapts Transformer (Vaswani et al. 2017) to

accurately forecast hydrological drought in the Apalachicola River.

Compared with other studies using limited features (Dikshit, Pradhan, and Alamri 2021; Khan et al. 2020), we consider more extensive features including physical conditions, climate conditions, and vegetation dynamics based on the underlying mechanisms of drought development. In particular, we consider the interplay between physical drivers and vegetation dynamics and advance our understanding of how climate and vegetation features and their spatial-temporal interactions regulate droughts. Thus we could learn more comprehensive representation from both static and temporal data to improve the forecasting performance. In addition, our method forecasts three different types of drought through multi-task learning using the shared representation without the need for extra computations to train separate models.

Time-series Forecasting Time series forecasting has been extensively studied across various domains, including climate science (Liang et al. 2023), traffic (Jiang et al. 2023), and healthcare (Kaushik et al. 2020). The complex and dynamic nature of time series data makes forecasting a challenging task. Depending on the forecasting length, time series tasks can be categorized into long-term and short-term forecasting. Additionally, based on data types, there are univariate, multivariate, and spatio-temporal forecasting. LSTM (Hochreiter and Schmidhuber 1997) has been widely used in many time-series forecasting tasks. Recently, due to the tremendous success of the Transformer in natural language processing and computer vision, it has also been widely adopted in time-series forecasting problems. Researchers have proposed many variants of Transformers, such as Informer (Zhou et al. 2021), Autoformer (Wu et al. 2021), FEDformer (Zhou et al. 2022), PatchTST (Nie et al. 2023), iTransformer (Liu et al. 2023). Even though some transformers are proven not effective as linear-based methods like (Zeng et al. 2023) in some tasks. The ability of Transformer to model global dependencies still makes them a popular choice for time series problems.

6.3 Addition Results

Variable Importance Comparison In this section, we quantify the importance of each attribute to prediction from the perspective of prediction accuracy. We train models by excluding the predictive features one at a time and measure the change in model loss at the first epoch compared to a baseline model that uses all features. The differences shown in Figure 7 illustrate the contribution of each feature to the performance of the models. The results also prove that static features such as vegetation dynamics and climate conditions are valuable in spatiotemporal forecasting for drought prediction tasks.

Ablation Study on Static Features In this section, we analyze the impact of each component within our model design. Initially, we assess the effectiveness of integrating static features into drought prediction tasks. To do this, we ablate the static features and compare *SPDrought* with the modified version (*SPDrought(t)*) that does not utilize static features. *SPDrought(t)* concatenates a full zero vector to the temporal representations before the transformer decoder and

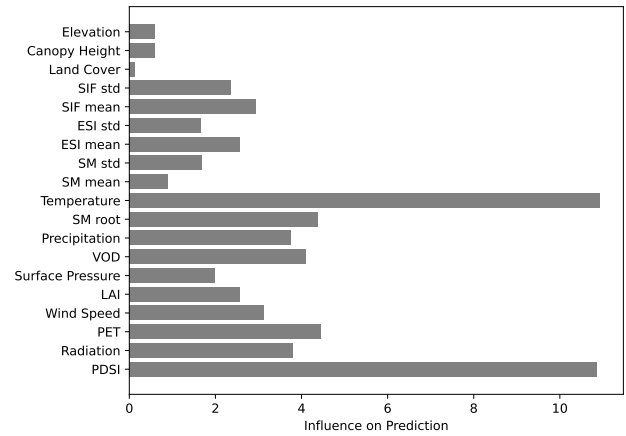


Figure 7: Relative Importance of Predictors

is also trained for 30 epochs. Then, we also investigate the impact of the spatial-temporal feature fusion module on model performance. So, we also conduct an additional experiment where we remove this module (denoted as *SPDrought(f)*) and present results in Figure 8. The results show that combining static predictors in representation can improve the forecasting performance across all drought prediction tasks, and the spatial-temporal feature fusion module consistently improves the performance and yields more stable outcomes.

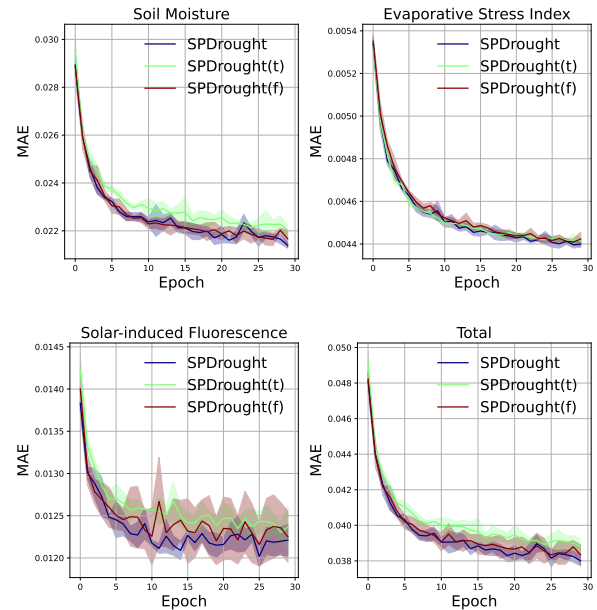


Figure 8: Ablation study on static features and spatial-temporal fusion module. We run the experiment three times and report the average MAE loss on the test set.

Ablation Study on Multi-task Training Here, we compare multi-task training with single-task training and report the results in Table 4. The ablation study highlights the ef-

Table 4: Average MAE of the ablation study on multi-task learning

Model	Soil Moisture	Evaporative Stress Index	Solar-induced chlorophyll Fluorescence	Total
SPDrought(Single)	19.39 \pm 1.26	3.35 \pm 0.22	10.50 \pm 0.45	33.24 \pm 0.93
SPDrought(Multi)	21.39 \pm 0.14	4.40 \pm 0.02	12.21 \pm 0.23	38.01 \pm 0.35

Table 5: Ablation study on model parameters

MAE ($\times 10^{-3}$)	SPDrought	SPDrought(w/o Encoder)	SPDrought(w/o Decoder)	SPDrought(50)
Soil Moisture	21.39 \pm 0.14	28.20 \pm 0.17	23.87 \pm 0.33	22.46 \pm 0.14
Evaporative Stress Index	4.40 \pm 0.02	5.51 \pm 0.01	4.72 \pm 0.04	4.51 \pm 0.01
Solar-induced chlorophyll Fluorescence	12.21 \pm 0.23	17.24 \pm 0.58	12.41 \pm 0.13	12.30 \pm 0.15
Total	38.01 \pm 0.35	50.95 \pm 0.70	41.01 \pm 0.48	39.27 \pm 0.06

Table 6: Average MAE over three runs of experiments on drought indices over 26 weeks using the temporal split

MAE ($\times 10^{-3}$)	SPDrought	Informer	PatchTST	DLinear	iTransformer	TimesNet	LSTM
Soil Moisture	47.77 \pm 0.58	51.97 \pm 0.09	48.27 \pm 0.28	48.66 \pm 0.81	49.55 \pm 0.12	48.48 \pm 0.21	53.61 \pm 0.16
Evaporative Stress Index	5.94 \pm 0.02	6.37 \pm 0.06	6.52 \pm 0.04	6.69 \pm 0.10	6.39 \pm 0.03	6.20 \pm 0.03	6.48 \pm 0.04
Solar-induced chlorophyll Fluorescence	22.26 \pm 0.05	25.91 \pm 0.18	29.16 \pm 0.47	29.28 \pm 0.38	25.28 \pm 0.15	25.27 \pm 0.59	26.04 \pm 0.20
Total	75.94 \pm 0.65	84.24 \pm 0.19	83.93 \pm 0.78	84.60 \pm 1.23	81.20 \pm 0.13	79.93 \pm 0.81	86.10 \pm 0.23

efficiency of the multi-task learning approach. While training the SPDrought model on multiple tasks simultaneously (*SPDrought(Multi)*), it achieves comparable results to training on individual tasks (*SPDrought(Single)*) but in about one-third the time. This demonstrates that multi-task learning can significantly speed up the training process without a substantial drop in accuracy, making it a valuable strategy when time and computational resources are limited.

Ablation Study on Model Parameters In this section, we explore the contribution of each component by removing the component from *SPDrought*. We conduct this study by creating variants of the model: *SPDrought* without the Transformer Encoder (*SPDrought(w/o Encoder)*), *SPDrought* without the Transformer Decoder (*SPDrought(w/o Decoder)*), and *SPDrought* with a reduced training window of 50 weeks, approximately one year (*SPDrought(50)*). These variants help us understand the role of each component in capturing temporal dependencies and learning drought patterns from historical data. As shown in Table 5, the Transformer encoder effectively helps to capture time dependence and thus significantly improves the overall performance. Furthermore, reducing the training window to 50 weeks (*SPDrought(50)*) slightly affects the model’s accuracy. It suggests that SPDrought can effectively learn drought patterns even with limited historical data. However, extended historical data contributes to better model performance, highlighting the importance of a more comprehensive dataset for training.

Comparison on Temporal Splitting In the previous comparison, we evaluate each method on test pixel regions. Here, we adopt a temporal split in the data, assessing the baseline methods and our approach for predicting drought indices over the next 26 weeks which are not seen during training.

Supplementary Results We present the Table 2 with standard deviations in the Table 8. We also include the accuracy and precision with standard deviations in Table 7, where we

report the significance of improvements using paired t-tests on precision.

6.4 Data Source

We collect data from the following source:

- NLDAS (Xia et al. 2012): NLDAS is provided by NASA, collected from <https://ldas.gsfc.nasa.gov/nldas>.
- SMAP (Das et al. 2018): SMAP is a public dataset provided by NASA, collected from <https://smap.jpl.nasa.gov/>.
- ALEXI ET was obtained upon request from Thomas R. Holmes and Christopher R. Hain on 28 January 2020 and was presented in (Holmes et al. 2018; Liu, Holtzman, and Konings 2021).
- CSIF (Zhang et al. 2018): CSIF dataset is under CC BY 4.0, collected from <https://figshare.com/articles/dataset/CSIF/6387494>.
- ERA5 (Muñoz-Sabater et al. 2021): ERA5 is provided by the European Centre for Medium-Range Weather Forecasts under Copernicus license, data collected from <https://www.ecmwf.int/en/forecasts/dataset/ecmwf-reanalysis-v5>.
- SRTM (NASA JPL 2013): NASA Shuttle Radar Topography Mission (SRTM) datasets are provided under the U.S. Geological Survey (USGS), collected from <https://lpdaac.usgs.gov/products/srtmgl1v003/>.
- VODCA (Moesinger et al. 2020): VODCA is under CC BY 4.0, collected from <https://zenodo.org/records/2575599>.
- MODIS (Myneni, Knyazikhin, and Park 2015): MODIS is provided by NASA, collected from <https://modis.gsfc.nasa.gov/>.
- GLAD (Potapov et al. 2021): Global Land Analysis & Discovery (CC BY), collected from <https://glad.umd.edu/>.

Table 7: Evaluation of drought prediction by soil moisture with standard deviations.

	SPDrought	Transformer	Informer	PatchTST	DLinear	iTransformer	TimesNet	LSTM
Accuracy	86.26 \pm 0.11	76.09 \pm 0.11	72.16 \pm 0.34	62.24 \pm 4.63	62.85 \pm 0.01	77.18 \pm 0.04	81.54 \pm 0.91	77.45 \pm 0.26
Precision	76.80 \pm 0.17	59.94 \pm 0.19	53.40 \pm 0.57	36.94 \pm 7.70	37.96 \pm 0.02	61.74 \pm 0.07	68.98 \pm 1.51	62.18 \pm 0.43
p-value	-	1.49 \times 10 ⁻⁴	9.96 \times 10 ⁻⁵	1.17 \times 10 ⁻²	6.78 \times 10 ⁻⁶	1.68 \times 10 ⁻⁵	9.77 \times 10 ⁻³	5.57 \times 10 ⁻⁴

Table 8: Average mean absolute error over three runs of experiments with standard deviations

MAE ($\times 10^{-3}$)	SPDrought	Transformer	Informer	PatchTST	DLinear	iTransformer	TimesNet	LSTM
Soil Moisture	21.39 \pm 0.14	34.56 \pm 0.24	38.08 \pm 0.14	36.32 \pm 0.19	47.61 \pm 0.04	32.34 \pm 0.09	25.96 \pm 0.46	31.36 \pm 0.40
ESI	4.40 \pm 0.02	5.99 \pm 0.07	6.37 \pm 0.06	6.37 \pm 0.00	6.82 \pm 0.01	6.06 \pm 0.01	5.11 \pm 0.02	5.83 \pm 0.09
SIF	12.21 \pm 0.23	16.00 \pm 0.23	17.71 \pm 0.33	21.36 \pm 0.19	20.99 \pm 0.03	15.47 \pm 0.07	14.11 \pm 0.03	15.35 \pm 0.02
Total	38.01 \pm 0.35	56.56 \pm 0.05	62.16 \pm 0.43	64.05 \pm 0.34	75.41 \pm 0.05	53.87 \pm 0.16	45.18 \pm 0.44	52.54 \pm 0.40

- NLCD (Homer, Fry, and Barnes 2012): Nation Land Cover Database is in the public domain, provided under USGS, collected from <https://www.usgs.gov/centers/eros/science/national-land-cover-database>.